Spring 4-6-2018

Application of Unmanned Aerial Systems (UAS) to Quantify Biomass, Stem Volume, and Basal Area in a Mature Norway Spruce (Picea Abies) Plantation in Central New York

Daniel Tinklepaugh
dmtinklepaugh@gmail.com

APPLICATION OF UNMANNED AERIAL SYSTEMS (UAS) TO QUANTIFY BIOMASS, STEM VOLUME, AND BASAL AREA IN A MATURE NORWAY SPRUCE (PICEA ABIES) PLANTATION IN CENTRAL NEW YORK

by

Daniel Tinklepaugh

A thesis
submitted in partial fulfillment
of the requirements for the
Master of Science Degree
State University of New York
College of Environmental Science and Forestry
Syracuse, New York
April 2018

Division of Environmental Science

Approved by:
Eddie Bevilacqua, Major Professor
Avik P. Chatterjee, Chair Examining Committee
Russell Briggs, Director, Division of Environmental Science
S. Scott Shannon, Dean, The Graduate School

ACKNOWLEDGEMENTS

I'd like to thank those who have helped me during my time as a candidate and ultimate recipient of a Master's Degree in Environmental Sciences during the past two years. To my advisor Dr. Eddie Bevilacqua, I am grateful for your ability to advise me on the proper course towards graduation while continuing his own work with classes, research, and advising other students. Your willingness to see value in my technical and academic skills is what enabled me to begin my work towards a higher degree. A sincere thank you to Paul Szemkow and his help in acquiring the specialized tools and equipment that were critical to the success of my work. To my temporary field assistants Joshua Ellison and Samuel Peterson, thank you for spending time gathering data and preparing the study area for many days at a time. Your company was consistently enjoyable and productive. Lastly, to my parents Dr. Pamela Cook and Dr. Mark Tinklepaugh, thank you for encouraging me to continue my work and supporting me as only parents can do.

TABLE OF CONTENTS

LIST OF FIGURES

LIST OF TABLES

Terms and Definitions

UAS – the combination of a UAV, RPC, GCS, and the payload (sensor or camera) attached to the UAV.

UAV – Unmanned Aerial Vehicle – Otherwise known as a "drone", these craft may be controlled directly or through a pre-programmed flight path.

RPC – Remote Pilot in Command – An individual licensed by the Federal Aviation Administration (FAA) to operate UAS safely and efficiently.

GCS – Ground Control Station – A controller and tablet combination that allows the RPC to control the UAV from a distance.

Spatial Resolution – Also known as Ground Sampling Distance (GSD), this is the measurement of an individual pixel in a single dimension (cm). Directly dependent on sensor width (m), focal length (mm), and flight height (m).

Spectral Resolution – Denoted as lowercase lambda (λ) and measured in micrometers (μm), this is the capturable wavelength on the electromagnetic spectrum for a sensor.

Radiometric Resolution – The range of values for an image, dependent on bit-depth of the sensor. For example the sensors used in this report were 8-bit sensor and therefore allowed 256 values for any band in a captured image.

Photogrammetry – The science of determining the exact positions of surface points and making measurements from photographs.

ABSTRACT

D. Tinklepaugh. Application of Unmanned Aerial Systems (UAS) to Quantify Biomass, Stem Volume, and Basal Area in a Mature Norway Spruce (*Picea Abies*) Plantation in Central New York. 55 pages, 3 Tables, 23 Figures. 2018

The focus of this study is to evaluate the applicability of low cost, commercially accessible UAS platforms, equipment, and techniques for forest inventory. This involved quantifying total aboveground biomass by: a complete field enumeration of aboveground biomass in a Norway Spruce (*Picea abies*) plantation, acquiring UAS imagery over the plantation, deriving indirect estimates of tree size distribution information from the imagery, then correlating imagery information with field biomass measurements. Results showed generally poor correlations between spatially explicit UAS-derived metrics and field measurements of forest biomass. Recommended refinements to UAS mission parameters to improve forest biomass estimation were detailed.

Keywords: Photo-interpretation, Geospatial, Remote Sensing, Allometry

D. Tinklepaugh
Candidate for the degree of Master of Science, May 2018
Eddie Bevilacqua, Ph.D.
Department of Forest and Natural Resources Management
State University of New York, College of Science and Forestry
Syracuse, New York

CHAPTER 1. INTRODUCTION

1.1. Importance of Quantifying Biomass

As an indicator of carbon content, biomass can be used to better understand forest ecosystem services, such as carbon sequestration, and may therefore be a crucial component in fighting the rise in greenhouse gas emissions (Nair et al., 2009). In other settings such as agriculture, biomass is most often used to quantify the amount of a crop that has grown as a fuel source.

The study area in question is a Norway spruce (*Picea abies*) planted in 1931 (Figure 1). The management of such plantations is performed manually, with timber cruises performed by a forester who takes samples of the population with regards to size and health. If more efficient methods of obtaining reliable estimates of the quantity of a crop in a plantation can be developed, then work load may be reduced on the forester.

Figure 1: A portion of the study area showing individual Norway spruce (*Picea abies*) trees.

1.2. Field Methods for Quantifying Biomass

Estimating tree biomass is generally performed by measuring diameter-at-breast height (dbh) or height (h) for use in allometric equations (Muukkonnen, 2007). These measurements may be applied to an allometric model to predict biomass yet are most useful if the model in use was developed adapted for the region, climate, or forest structure of the study population. In this study I prioritized allometric models whose study populations (those used to prepare the allometric equation and scaling coefficients) included Norway spruce of comparable size to those found in North Compartment 40.

1.3. Allometric Models

Allometry is the estimation of certain metrics, such as height or mass, based on measurements from a different part of the same organism. Often in the form:

$$Y = aM^b \quad (1)$$

where Y represents a biological variable, M a measure of body size, and b a scaling exponent (Gittleman, 2011). Scaling coefficients, or exponents, vary between reports and are applied by the user for cases in which choosing between mass, volume, or even system of measurement are in the user's interest. In my case, the predicted dimensions are mass and volume for the entire Norway spruce trees whose dbh has been measured in the field. Basal Area was calculated using simple geometric conversions of diameter to cross-sectional area.

1.4. Remote Sensing in Forest Inventory

1.4.1. Historical Role of Aerial Photographs in Forest Inventories

Remote sensing in forest inventory began in the early 1900's with cameras mounted to the fuselage of an aircraft or held by an operator. The film used was almost exclusively analog panchromatic black and white, supplemented a few decades later with Kodachrome color prints and early infrared imagery. Such techniques allowed foresters to better understand their study areas and continued in use until the early 2000's as a functional tool in forest classification techniques (Franklin et al., 2010).

Photogrammetry is the study of taking measurements from photographs and its use in surveying is dependent on high precision, understanding sensor variables (such as focal length and width), the geometric relationship of the camera to the subject, and more. In the past, the

distinction between photogrammetrists and foresters wishing to apply aerial photographs to their work was strong, with foresters focusing not so much on precision but the ambiguous nature of stand boundaries and forest canopies. Their priorities, however, were cost per image (measured in cents/acre) and covering their study area during leaf-on periods (Spurr, 1946).

As digital imaging technologies became more available in the past two decades, multispectral and hyperspectral imaging enabled the user to gather a wide range of usable data in formats more amenable to computer-based analysis.

1.4.2. Potential Benefits of Unmanned Aerial Systems over Airborne Remote Sensing

Unmanned Aerial Systems (UAS) have overcome the disadvantages of airborne remote sensing techniques (e.g., high cost, low spatial resolution, poor temporal resolution, etc.) and are more flexible (Siebert & Teizer, 2014). Even if one does not own their own UAS and must hire a flight contractor, planning and executing missions takes mere minutes. Additionally, to be able to adjust one's payload to mission specifications with different mountings or sensors is simple and offers the user greater control over the data capture process than traditional platforms. They are a low-cost alternative to classical manned aerial photogrammetry and their application to civilian purposes has followed their initial development in military spheres of influence (Remondino et al., 2011). Their ability to survey a location with little delay in high resolution at an affordable cost is undoubtedly a major advantage over traditional remote sensing techniques or field data measurements. Additional uses for drones in terms of natural resources management include canopy mapping, measuring forest canopy height, tracking wildfires, and supporting intensive forest management (Tang & Shao, 2015).

1.4.3. Short History of Environmental Application of UAS

Similar to site specific crop management (SSCM), precision farming depends on advanced sensor systems to measure environmental variables with which one may optimize crop output with the resources available. For example, a Normalized Difference Vegetation Index (NDVI) may be produced to determine locations of stress on any green, leafy crop. An NDVI is a numerical indicator of healthy green vegetation that exists in an area and provides a valuable indicator of photosynthetically active vegetation by comparing emissivity in the Photosynthetically Active Radiation (PAR) spectral region (0.4 to 0.7 μm) to that of infrared (0.7 to 1.1 μm). Because plants absorb PAR and reflect infrared, as infrared radiation is unfit to produce organic molecules and would only serve to overheat the plant, one can detect the presence of green vegetation by finding those areas in an NDVI image where the difference in values is greatest (Pettorelli et al., 2005).

Well suited to hovering at low altitudes and maneuvering within a dangerous environment, UAS have also been used in search and rescue operations where exploration by foot is unfeasible or the search area is too large to be covered by a team on the ground. Most importantly, the availability of highly accurate and low-cost Global Positioning Systems (GPS) enables these craft to maintain and record their position nearly anywhere on Earth (Seibert & Teizer, 2014). As time is critical in search and rescue, the physical agility and ease of preparing for flight missions associated with UAS provide rescuers with the ability to survey areas in which lost persons may be located. Still images and videos may be transmitted to a ground control system (GCS) for processing by human rescuers and anomalies analyzed for their likelihood of being the endangered individual (Waharte & Trigoni, 2010).

1.4.4. Typical UAS Platforms

UAS offer researchers the ability to gather data in fine spatiotemporal resolution with no need to pay for individual scenes, deal with low resolution, or the possibility of cloud cover obscuring the study area. UAV come in two distinct packages: fixed wing and multi-rotor variants (Figure 2). Fixed wing craft have superior range, velocity, and are well-suited to covering huge tracts of land (Everaerts, 2008). Wingless craft are often found in quadcopter (four rotors) with some models using up to eight at the same time (Anderson & Gaston, 2013).

Figure 2: Multirotor copter (left) and fixed wing (right) Unmanned Aerial Vehicles.

1.4.5. Other Considerations – FAA Regulations

In order to properly gather aerial data, it is important that one understands the regulations dictating the use of their unmanned craft in terms of legality and flight capabilities. The use of UAS in the United States is controlled by the Federal Aviation Administration (FAA) under the *Drone Operation and Certification Regulations* – Title 14 of the Code of Federal Regulations Part 107, also known as 14 CFR § 107 (FAA, 2016). A small unmanned aircraft is defined as any unmanned aircraft weighing less than 55 pounds on takeoff, including anything

attached to the aircraft. It is a component of a small unmanned aircraft system which includes all elements required for safe and efficient flight. These include the remote pilot in command (PIC), ground control system (GCS), and the craft itself (FAA, 2016). While available to the public as a tool for recreation and research, their use is dictated primarily by altitude limitations, proximity to clouds, flyover restrictions, and how heavy the craft is during flight. These limitations are: one cannot fly 500 ft (152.4 m) beneath or within 2500 ft (762 m) horizontally to cloud cover, the craft must weigh less than 55 lbs (24.95 kg), the craft cannot fly greater 400 ft (121.92 m) above the terrain or the highest point of a structure beneath it, and one cannot fly over individuals who are not participating in the flight mission with proper safety equipment (FAA 2016).

To prepare for flight missions, a takeoff and landing site needs to be prepared: first, one should choose an open area with no canopy within approximately 10 m (low shrubs and grasses directly adjacent to the landing site should be flattened or cut away) that is within a short distance to the study area so as to reduce excess battery consumption. During takeoff it is advisable to keep the craft on the ground during high winds. These precautions prevent the likelihood of UAS collision with trees and improve the navigation system's connection to satellites immediately before takeoff. In my experience, if the UAS cannot connect with enough satellites to determine its location, in the case of pre-planned missions, it will not takeoff.

CHAPTER 2. GOALS AND OBJECTIVES

Goal: The overall goal of this research is to evaluate the potential application of low cost, commercially accessible Unmanned Aerial System (UAS) platforms to forest inventory.

Objectives:

Specific objectives that needed to be accomplished to meet the research goal included:

1. Conducting a complete enumeration and measurement of every mature Norway spruce within the study area;
2. Perform aerial missions over the study population using a UAS to collect aerial stereo imagery;
3. Convert acquired aerial imagery into useful forest inventory data; and
4. Correlate imagery data with field measurements to assess its accuracy and distribution.

CHAPTER 3. METHODS

3.1. Field Site

The study area used in this research is a Norway spruce plantation in Svend O. Heiberg Memorial Forest, just south of Onondaga County in Central New York (Figure 3). Svend O. Heiberg Memorial Forest is managed by the State University of New York College of Environmental Sciences and Forestry (SUNY ESF) for educational, commercial, and recreational purposes. The entire forest covers approximately 15.4 km^2 in total and rests between the towns of Tully and Truxton, with a very small portion extending north into Tully and Fabius townships (Figure 3). North Compartment 40 was chosen for study because of its homogeneity of age and species. The compartment was planted in 1931 by the Civilian Conservation Corps, which excluded the necessity of categorizing groups within the population. Approximately less than 1% of mature trees in the stand were not Norway spruce. While homogeneous in composition, past management has removed the typical uniform spacing found in tree plantations, creating a partial irregular spacing between trees.

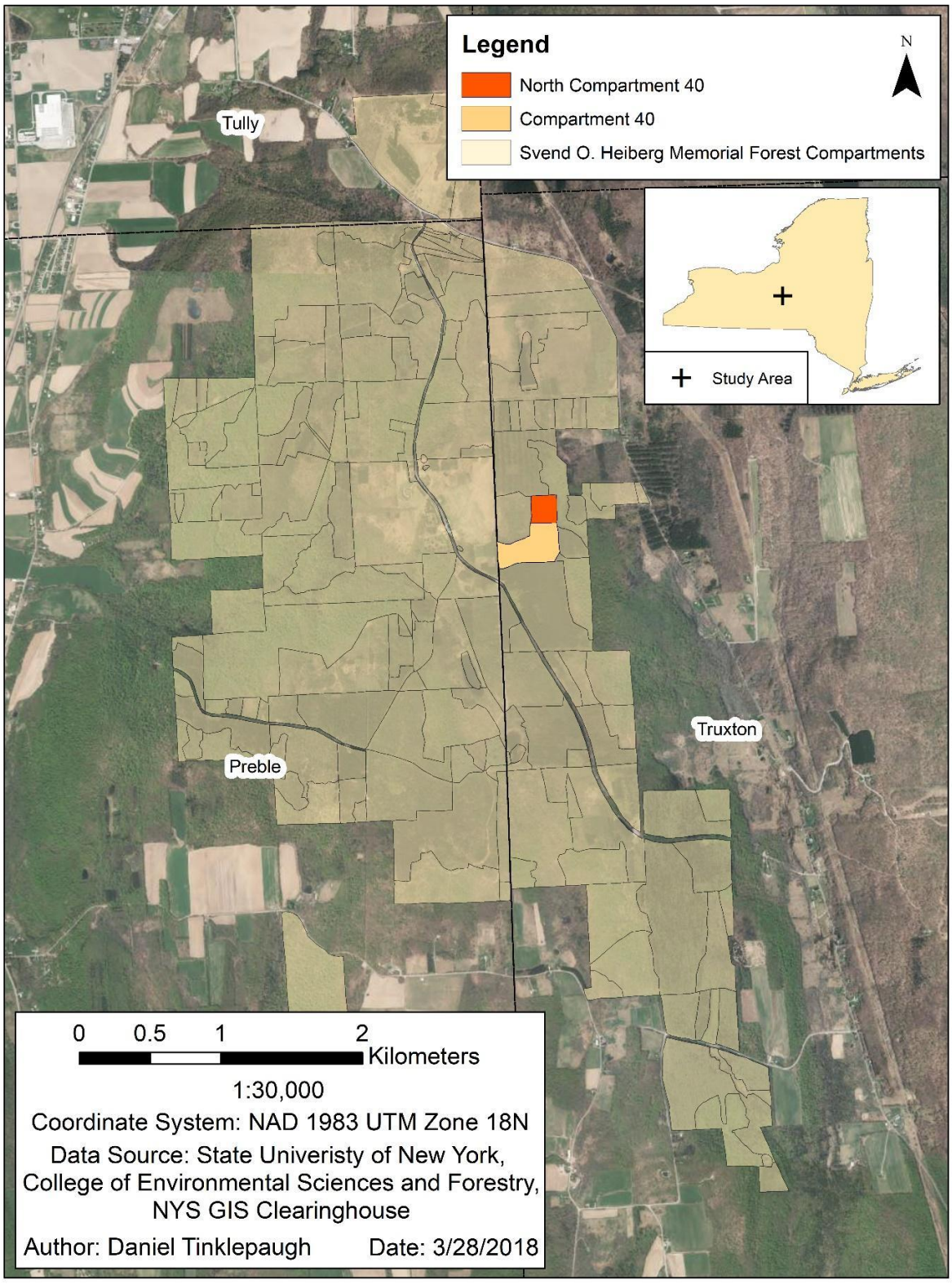

Figure 3: Location of study site (North Compartment 40) within Svend O. Heiberg Memorial Forest in Central New York.

3.1.1. Early Use of INTERPNT

INTERPNT is a free software package produced at Harvard University in 1997 as a tool for foresters with which to produce accurate maps of trees solely with tree diameter and tree-to-tree distance measurements (Boose et al. 1998, 1999). INTERPNT applies the principles of trilateration, or coordinate determination using three distance measurements from points whose locations in space are known to place an unknown point in a two-dimensional space, to forest inventory. Because one cannot measure from the exact center of a tree, the diameter-at-breast height (dbh) of the individual must be measured such that its radius may be added to a distance. INTERPNT was designed to determine the location of Tree D based on distance measurements from Trees A, B, & C, including their dbh. To improve organization and ease of use, I decided to use colored stakes (Figure 4) in lieu of actual trees for A, B, & C. Because of this, I input the dbh of these markers into INTERPNT as 0 cm as I could measure from the direct center (above the stake) to any one tree in visual range. While very well suited to perform its initial task, INTERPNT is difficult for a single person to perform for a study area as large as mine with unreliable Cartesian coordinates for even the control stakes. Due to the dubious utility of inaccurate geolocation from this approach, plus the amount of time needed to perform this task for the whole study area, I decided to drop INTERPNT completely and instead simply measure tree dbh and designate in which plot the tree resided. I recommend that anyone attempting to use INTERPNT in the future do so in an open area such that a plot marker's location may be determined from orthoimagery or a GPS unit with no canopy overhead or produce their own grid coordinate system without the use of GPS.

3.1.2. Laying Out Plots

Enumeration of the study area was performed in the autumn of 2017 and took approximately one month. This included laying out inventory plots with painted stakes (Figure 4), geolocating said stakes with a GPS (Figure 5), measuring the dbh of every mature Norway spruce using a diameter tape (Figure 6), then flying aerial missions with a UAS over the study area (Figure 7).

Figure 4: Example of stake used to mark corner of inventory plot within North Compartment 40.

Beginning at the Northwest corner of North Compartment 40, 90 plots were originally laid out in a rough North – South and East – West grid pattern with

Figure 5: Image of Trimble Geo XH 3000 GPS unit used to geolocate inventory plots corner stakes.

Figure 6: Image of diameter tape used to measure diameter-at-breast height (DBH, cm) on Norway spruce trees

Figure 7: (Left) The underside of the 3DR Solo fitted with three cameras. (Right) The ground control station (GCS) and the unmanned aerial vehicle (UAV) which together constitute a complete unmanned aerial system.

vertices marked with painted stakes (Figure 4). Plots were numbered from 1 to 90. A tripod-mounted Trimble Geo XH 3000 GPS unit (Figure 5) was used to gather more than 100 points over each marker with the antenna extended to 3 m above the forest floor. Complete enumeration of each Norway spruce in each plot was conducted with two measurements collected per tree; its dbh and residence in one of 90 Inventory Plots. After consideration, it was decided that final analyses would be performed exclusively for data gathered on the interior plots – i.e., not using any of the plots that bordered of the study area (Figure 8). Further explanation of this decision may be found in the discussion section.

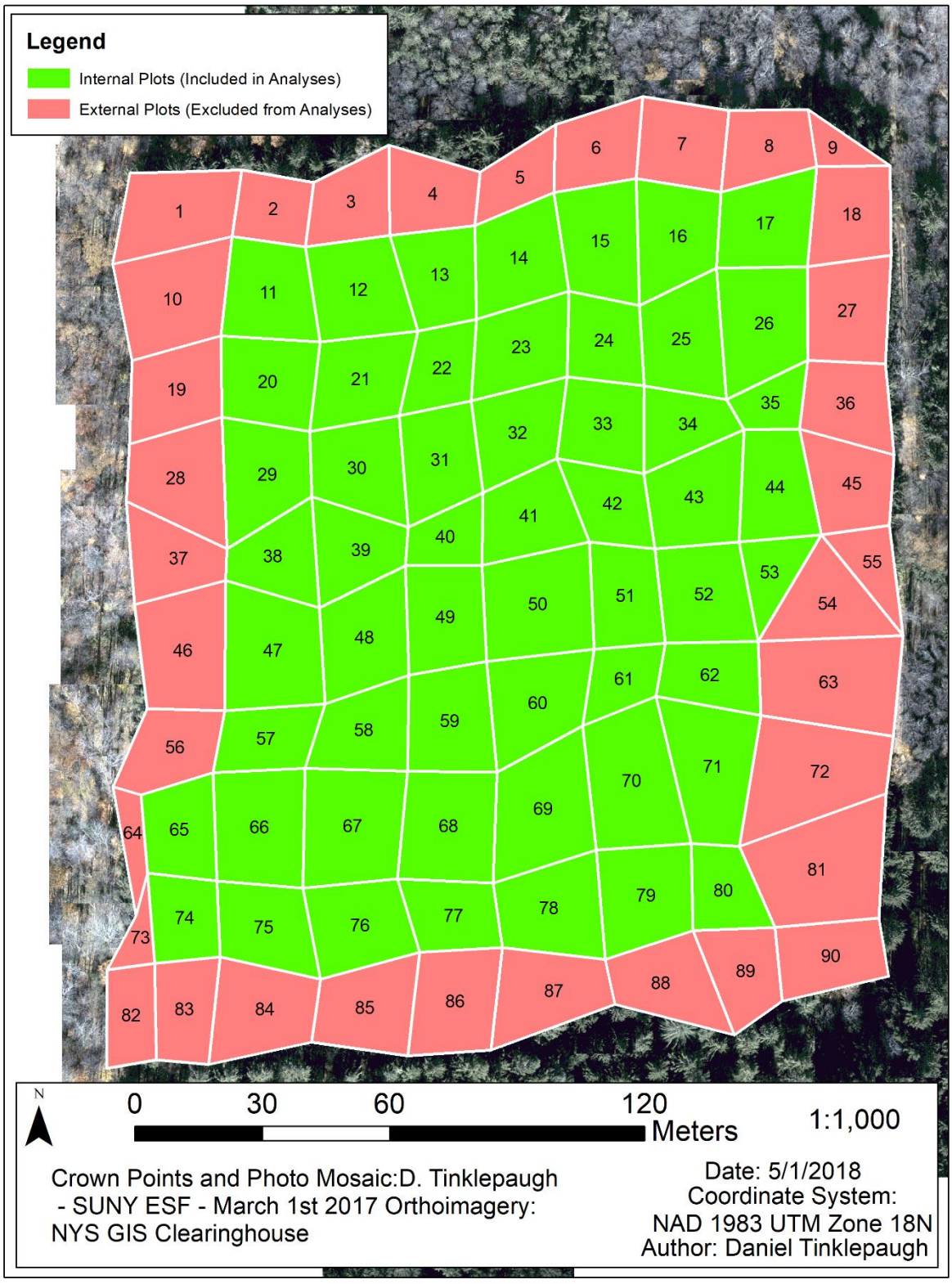

Figure 8: Inventory Plots for North Compartment 40. Both internal and external plots were used in initial analyses, and while only internal plots were used during final analyses. Numbers indicate Plot ID value. White lines delineate borders.

3.1.3. Individual Tree Selection and Measurements

Any tree whose base was located on the boundary between two plots was always associated with the plot which contained greater than 50% of its base. With the aid of an assistant, each plot was inventoried, during which as I would measure trees, state their dbh, and mark said tree with tape to avoid measuring the same individual twice.

3.1.4. Tree Volume & Biomass Estimates

3.1.4.1. Volume

Developed in a study intended to cover the five major tree species in Europe (*Picea abies, Pinus sylvestris, Betula* spp., *Fagus* spp., and *Quercus* spp.), the following equation was used to calculate volume (m^3) for each Norway spruce tree in this research (Muukkonnen, 2007):

$$Y_i = \exp (B_0 + B_1 * \text{dbh} / (\text{dbh} + B_2)) \quad (2)$$

where Y_i represents volume (m^3) or mass (kg) of tree component *i* and dbh is diameter-at-breast height (cm). The model coefficients B_0, B_1, and B_2 vary depending on if the user wishes to calculate mass of the total aboveground, stem, foliage, or volume of the total tree (Muukkonnen, 2007). Because the above equation was prepared from a population of trees with dbh's ranging up to 60 cm, I find that this equation is likely to accurately predict the volume of even the largest trees (up to 68 cm) in my study.

3.1.4.2. Biomass

Biomass was calculated using an equation developed from a population of 30 trees ranging from 11.9 to 43.7 cm, destructively sampled in the Allegheny Plateau of Central New

York (Jokela et al., 1986a). While my population contained a range of individuals with dbh's of 13.3 to 68 cm and is a thinned stand, the proximity of the study area used to prepare the above equation hints at its suitability for use in my study area in a neighboring region of New York State.

The biomass equation is as follows:

$$Y_i = \exp(B_0 + B_1 \ln(dbh)) \quad (3)$$

where Y is dry weight (kg) of tree component i and dbh (cm) as previously defined, B_0 and B_1 are coefficients whose value depends on whether the user intends to model the mass of the stem wood, stem bark, foliage, live branches, dead branches, or total aboveground biomass (with or without dead branches). In my case, I choose to model the total aboveground biomass including dead branches in order to account for the total carbon content of Norway spruce in the study area.

3.1.4.3. Basal Area

Basal area was calculated using a simple geometric conversion of diameter to cross-sectional area.

$$BA = (\pi * (dbh / 2)^2) / 100 \quad (4)$$

where BA is basal area (m^2) of the tree and dbh (cm) as previously defined.

3.2. Unmanned Aerial System

3.2.1. Platform

Originally purchased to measure NDVI over willow crop in Central New York, our UAS consists of a 3DR Solo Quadcopter, three MAPIR Cameras (MAPIR 2018), an Asus Minitablet and Solo Ground Control Station (GCS) (Figure 7).

3.2.2. Payload

Mounted beneath the UAS were three MAPIR Survey 2 cameras (Figure 7) from which the visible spectrum (RGB), Red (R), and Near Infrared (NIR) band images were collected (MAPIR 2018). I chose the multispectral route as (a) the cameras were already mounted and ready to use for another project and (b) having non-visible wavelengths may have been useful in the case that multispectral analyses were desired.

3.2.3. Mission Planning

All missions flown in this study used a mission planning app called TOWER (DroidPlanner Labs, 2016) to guide the UAV during flight, This app runs on any android tablet, allowing the user to modify flight parameters, such as elevation (200, 300, and 400 ft) and neighboring image overlap (70%), which were the only two modified for this research. The remote pilot in command (PIC) was able, at any time, to pause the mission flight or cancel the mission by calling the UAS back to the takeoff site. Other parameters, such as maximum flight velocity (10 m/s), stabilization preferences, etc., were left at default values. Additionally, in the event that adverse weather conditions, extreme distances, or obstructions impeded radio connection between the controller and the UAS, preplanned missions are able to continue without issue and return to the operator when completed.

Because UAS in the United States are not permitted to fly above 400 ft above the terrain and the canopy beneath reached to approximately 100 ft, it was decided to fly three missions at different altitudes (i.e., 200, 300 and 400 ft). This would produce images at the lowest and highest recommended limits of distance between the UAS and the canopy. Lower altitude missions had to fly a longer path as the size of the study area remained the same (Figure 9) but were able to have small spatial pixel resolutions (Table 1). In the end, only 52 of the 72 RGB images from the 400 ft mission (Figure 10) were used in subsequent analyses in order to reduce the time needed for georeferencing and processing.

Figure 9: Flight paths of aerial missions surveys over North Compartment 40 at altitudes of 200 ft (left), 300 ft (center) and 400 ft (right).

Table 1: Detailed information concerning aerial missions flown above the study area – North Compartment 40 at Svend O. Heiberg Memorial Forest.

Height above ground (ft)	Date Flown	Mission Duration (min)	Total Number of Images	Pixel Resolution (cm)
200	October 25th, 2017	19	131	1.2
300	October 19th, 2017	9	109	2.4
400	October 25th, 2017	7	72	3.5

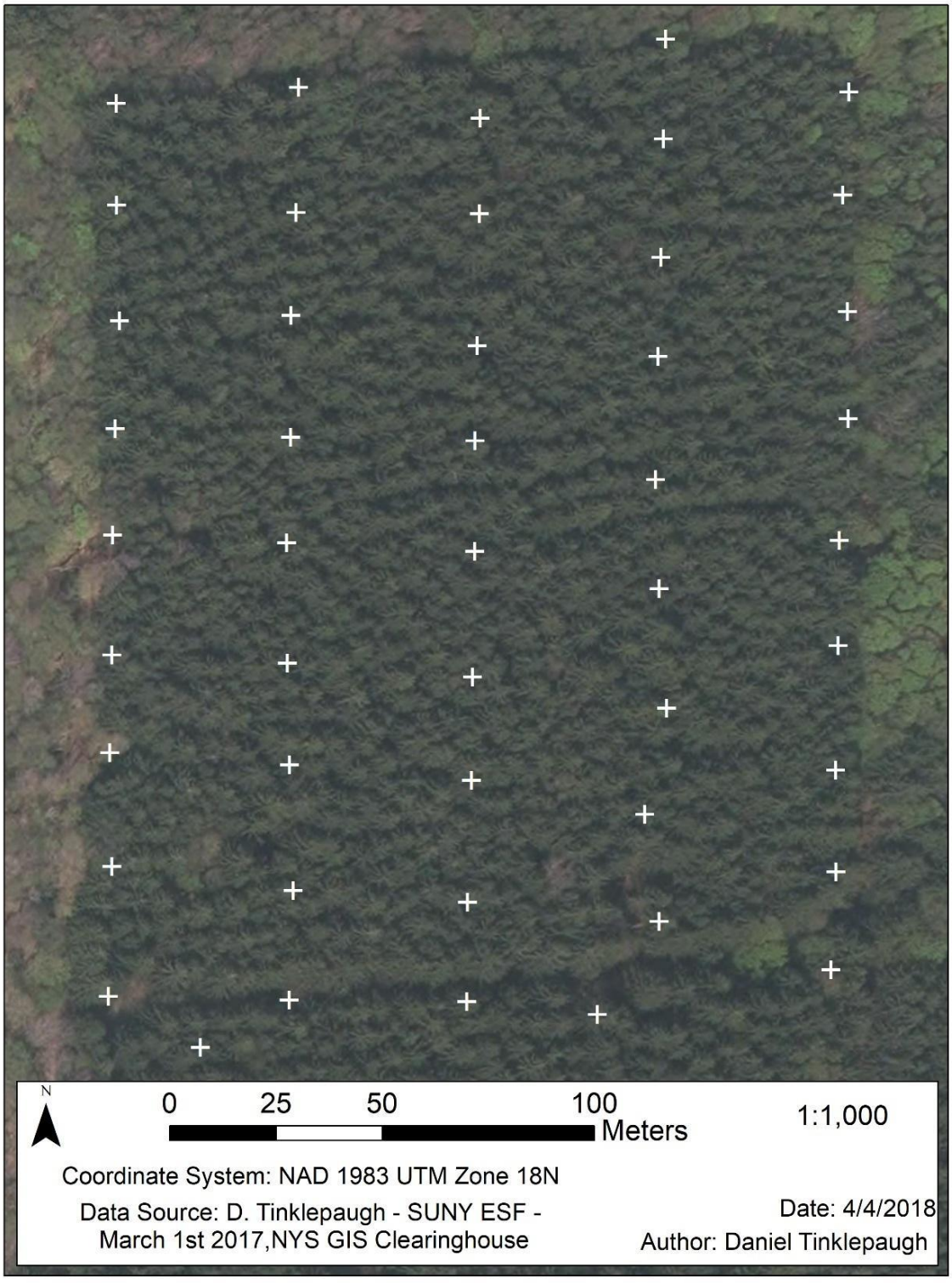

Figure 10: Center points (displayed with + symbol) of 52 geotagged images collected during October 25th mission when UAS was flown at an altitude of 400 ft above the ground.

3.2.4. Mission Summaries

All missions were flown on sunny days in late October in the early afternoon. The strategy was to reduce the size of the trees' shadows and have as much of the canopy illuminated as possible, yet the solar elevation angle was close to 35 degrees from the horizon for all missions. Cloud cover was sparse and wind speed was low, with gentle gusts. Instrumentation to measure these variables was not available. Ideal conditions for flight missions would have been at noon in the early summer, near the summer solstice, when the sun has the greatest angle of insolation for this latitude (around 72 degrees from the horizon), and light overcast conditions to provide diffuse, consistent lighting with as few shadows as possible.

Battery usage was about the same for all flights, with batteries nearly completely drained during return to takeoff. This was the result of low altitude missions requiring more passes over the study area (Figure 9), whereas higher altitude flights were exposed to higher wind speeds and therefore had to expend more energy fighting turbulence.

3.2.5. Mosaic Creation

A mosaic using 52 georeferenced images taken at 400 ft was produced in order to provide a continuous coverage of the study area from which tree crowns were geolocated (Figure 11). This step was done using the program ERDAS IMAGINE's 2D MosaicPro suite (ERDAS 2014). ERDAS IMAGINE is an image processing software package that enables the user to process geospatial and non-geospatial imagery, as well as vector data.

The 52 images went through three steps before georeferencing;

Step 1 - geotagging in GeoSetter (Schmidt 2011);

Step 2 - conversion from JPG to TIFF in MAPIR QGIS plugin; and

Step 3 - removal of coordinate system by opening every TIFF in MS Paint then saving each image to a folder.

Step 3 needed to be performed as it was discovered that by Geotagging my images and then converting to TIFFs, they effectively became GeoTIFFs and, therefore, could not be georeferenced in ArcMap. By opening the GeoTIFFs in MS Paint then saving them to another folder, this would remove the Exif metadata GPS coordinates and allow the images to be processed properly and rubbersheeted to their correct position.

3.2.5.1. Geotagging

Geotagging is the process of applying geographic coordinates and altitude to an image. This is sometimes performed by the camera itself when the image is captured, but in our case, was done at a later date. A free program known as Geosetter (Schmidt 2011) was used to assign these values to one or more images with or without a telemetry log. Telemetry logs serve as guides for Geosetter to follow, but one can manually designate coordinates by simply dragging a marker around the orthoimagery interface, then confirming that the coordinates at which the marker lies should be written to selected image(s). Because manually geotagging each image with its known location during capture would have been terribly time consuming and imprecise, it was discovered that using another free program called Mission Planner (ArduPilot Dev Team 2017) enabled the user to convert telemetry logs (which contain data such as time, date, location, altitude, and orientation of the craft at certain times) into GPX files;

readable by Geosetter as the path for which the images should be tagged upon. After conversion, the user chooses a point in time on the GPX path and corresponding image. It is possible to assign such values to a whole set of images of the same mission because the user designates the rate of image capture (3 seconds in our case) with which Geosetter calculates which images should be assigned to which points along the telemetry path. Geosetter then writes the altitude, location, and coordinate system into the image metadata. To reduce error, it is recommended that one go through the geotagged images to ensure that image metadata was properly rewritten.

3.2.5.2. Georeferencing

Georeferencing the 52 TIFFs was done by matching individual UAS images with New York State orthoimagery from New York State Geospatial Information System (NYS GIS) Clearinghouse in ArcMap (ESRI 2018). Georeferencing is the process by which the user designates the location of one point on the image being georeferenced to be "rubbersheeted" with that on a reference image and may be repeated several times to improve the fit of the modified image. Rubbersheeting is a term used to describe the distortion of an image to seamlessly join or match adjacent/overlapping imagery. Once the user is satisfied with the fit of the modified image, the newly shaped TIFF has its internal coordinate system associated to terrestrial geographic coordinates.

3.2.6. Photogrammetric Analysis for Creating 3D Point Cloud from Stereo Images to Estimate Crown Volume

One approach considered for this project was to generate a 3D point cloud from stereo images using a variety of available photogrammetry software program, including DroneDeploy

(DroneDeploy 2018), WebODM (WebODM 2018), Pix4D (Pix4d 2018), and AgiSoft Photoscan (AgiSoft Photoscan 2016). The idea was to extract useful biometrics such as height and crown volume from such a model. However, my imagery was poorly adapted to produce 3D outputs from stereo images and it was decided to abandon this approach in favor of working solely with 2D models.

3.2.7. Producing a Mosaic

Mosaics are combinations of neighboring images stitched together to produce a seamless aerial coverage for large areas. Whole orthoimagery of neighboring areas are sometimes captured in different seasons, the near-perfect continuity of orthomosaics is what distinguishes them from image mosaics, used in this thesis. ERDAS IMAGINE's 2D Mosaic Pro suite does enable the user to manually stitch neighboring images together, but this process is adapted for use with images taken from a more stable platform than mine so was therefore too time consuming and ditched in favor of an automatic mosaic production.

3.3. Photo-interpretation of Tree Counts from Mosaic

After processing in ERDAS IMAGINE (ERDA 2014), the image was brought into ArcMap (ESRI 2018). Next, a new shapefile was prepared in the form of points. This process was done manually by myself, in which I visually located the crowns of every tree that was visible in the mosaic. These points would represent identifiable tree crowns and were manually placed for the entire study area in under an hour (Figure 11).

Figure 11: Stem map produced for North Compartment 40 by manually locating tree crowns from a mosaic. Crosses indicate the perceived locations of tree crowns. 846 individuals in total were counted using this method.

3.4. Thiessen Polygon Generation

Thiessen polygons, also known as Voronoi polygons, are polygons whose boundaries define the area that is closest to each point relative to all other points. Their edges are the perpendicular bisector of lines at the midpoint between two points, with points representing tree crown peaks. The application of such geometry to crown growth space is a measure of point density in which area is the index variable and growth space/crown area are not yet known (Avery and Burkhart 1983, Brown 1965, Ford and Sorrensen 1992). Each tree has a point location from which Thiessen polygons are produced to determine maximum crown extent. They were applied in this thesis using ArcMap tool (ESRI 2018) to quantify tree crowns because manually delineating the area of each crown with a circle tool would have been imprecise and time consuming. I allocated the centroids of each Thiessen polygon to its resident Inventory plot because denoting plot crown area in a 100% canopy cover study area would not properly distinguish a tree's metrics to its resident plot and, therefore, provide more accurate census statistics for our test environment (Figure 12).

3.4.1. Correlation and Regression Analysis

Relationships between field measurements and quantitative imagery derived metrics at the plot level were visually assessed using scatter plots and analyzed using correlation and linear regression analyses (Minitab 2018).

CHAPTER 4. RESULTS

4.1. Tree List and Size-Class Distribution – Summary by Plots

A total of 1,532 mature Norway spruce individuals were located and measured in the study area (Figure 12). Of these, 909 were contained within the core 55 plots with a mean dbh of 38.13 cm with a standard deviation of 8.87 cm with an approximately normal distribution (Figure 13). A bell-shaped symmetrical distribution is evident because the study area is a plantation, in contrast to a negative exponential distribution often seen in natural forests.

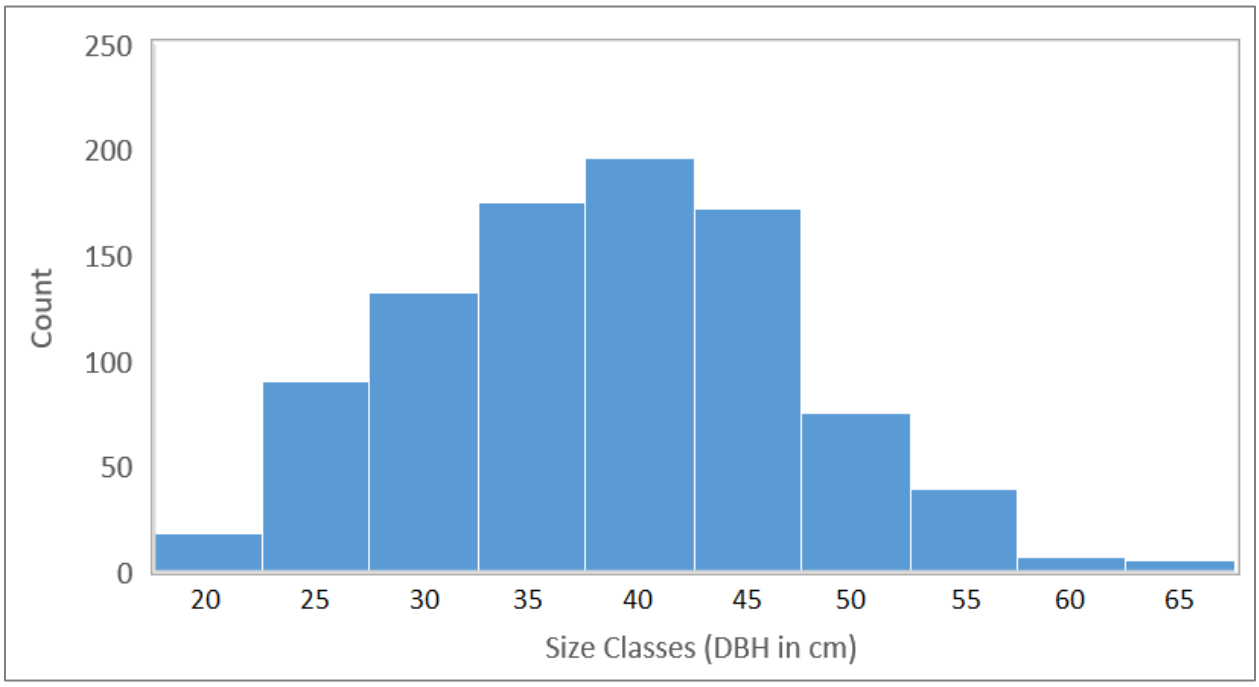

Figure 12: Size class (diameter-at-breast height, DBH) distribution of 1532 Norway spruce individuals in North Compartment 40. Mean = 37.77 cm and std. dev. = 8.95 cm.

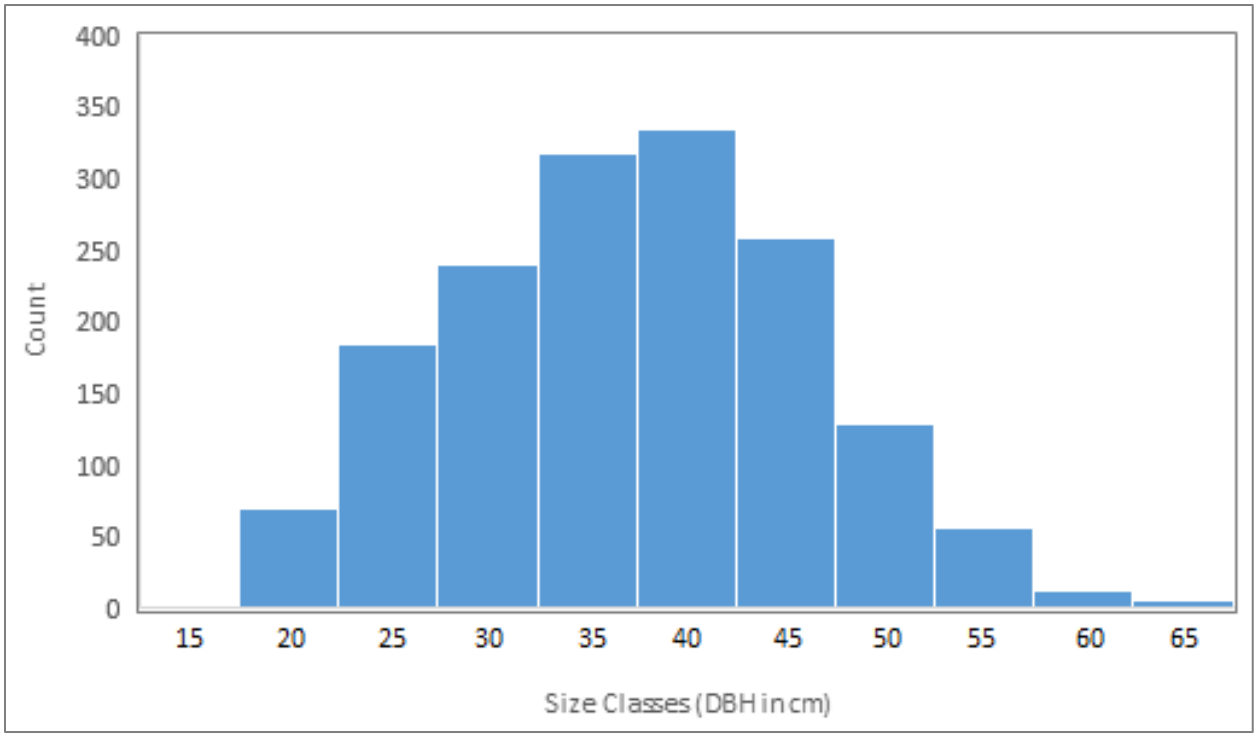

Figure 13: Size class (diameter-at-breast height, DBH) distribution of 909 Norway spruce individuals in North Compartment 40. Mean = 38.13 cm and std. dev. = 8.87 cm.

4.1.1. Basal Area, Volume, and Biomass by plot

Using the full census of trees from the 90 interior plots and equations (2) to (4), the cumulative basal area, volume and biomass of trees within each was obtained. Individual plot totals are available in Appendix. Summary statistics describing the distribution of plot totals (Table 2) indicate relatively homogeneous levels of tree occupancy within the plots, with basal area, volume and biomass having low coefficients of variation between 26 and 38%.

Table 2: Plot summary statistics from field and photo-interpretation measurements for North Compartment 40 Norway spruce.

Data collection method	Population	Measurement	Min	Mean	Max	Std. Dev	Total
Field	All n = 90 plots	Count (#)	3.00	17.02	42.00	6.52	1,532.00
		Basal Area (m^2)	0.33	2.02	4.70	0.68	181.40
		Volume (m^3)	3.62	21.80	51.09	7.34	1,962.30
		Biomass (tons)	2.03	12.23	28.65	4.12	1,100.60
	Interior n = 55 plots*	Count (#)	6.00	16.53	42.00	5.44	909.00
		Basal Area (m^2)	0.96	1.99	4.03	0.52	109.40
		Volume (m^3)	10.14	21.51	43.65	5.60	1,183.10
		Biomass (tons)	5.70	12.07	24.46	3.14	663.60
Photo-interpretation	All n = 90 plots	Count (#)	1.00	9.40	29.00	4.22	846.00
		Thiessen (m^2)	--	--	--	--	--
	Interior n = 55 plots*	Count (#)	3.00	9.71	29.00	3.98	534.00
		Thiessen (m^2)	19.75	47.60	82.75	10.13	2,618.15

*Used in subsequent regression analyses.

4.1.2. Thiessen Polygon Area

Exported Thiessen polygon areas available in Appendix. See Table 2 for Summary Statistics.

4.2. Mosaic

A 2D mosaic was produced for the entire study area (Figure 14).

Figure 14: Mosaic image produced using 52 stereo images collected from UAV flown at an altitude of 400 ft above the ground.

4.2.1. Individual Tree Size

4.2.1.1. Failure to Create 3D Point Class

After discussion with colleagues, it was decided that a major drawback in surveying the Norway spruce plots was the ubiquitous similarity between nearly every image. 3D imaging from stereo pair images works best when distinct cover features such as open spaces or roads exist in the surveyed area to provide the automated program with identifiably unique cover features. Additionally, neighboring images at lower altitudes did not always capture the same side of any one tree. I suspect that this was because the close proximity of the canopy to the UAS provided too much parallax distortion, or the displacement of an object between two images taken at different locations.

Looking at the mosaic produced by Drone Deploy as a secondary file during 3D model production (Figure 15), it is quite clear that not all of the images are properly oriented in any one direction. Since all aerial missions were flown on sunny days, the orientation of the images is quite clear based on the sun lit faces on the tree crowns and there seems to be no pattern concerning the orientation of the lit faces in the images. While the images used in this analysis were geotagged, the program seemingly reoriented the images when prioritizing shared cell values. Ground Control Points (GCP), used to help the program reliably recognize the cartesian location of a pixel on one image and thereby properly orient said image, may help but I feel as if one would need two per image to reliably orient the output model.

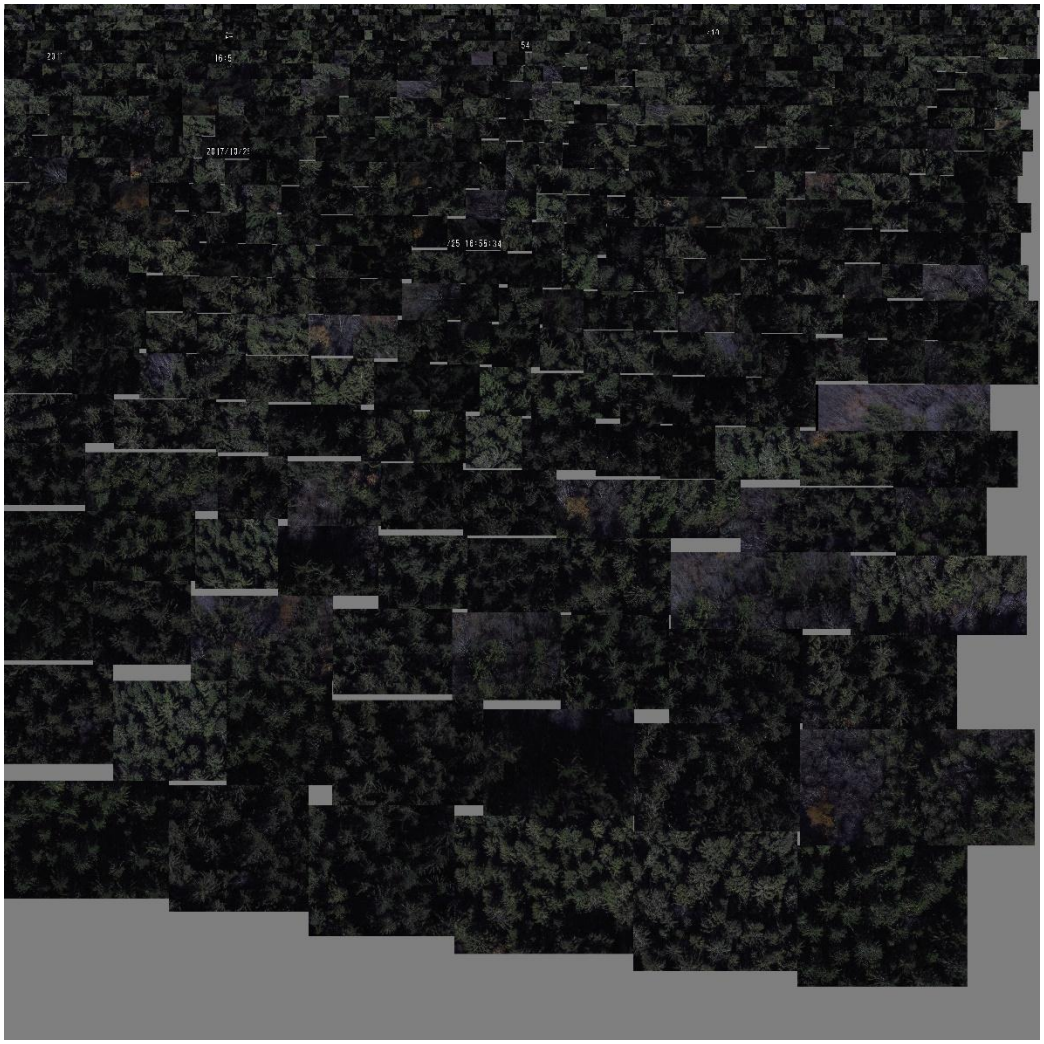

Figure 15: Mosaic image produced by DroneDeploy based on 52 stereo images collected from UAS flown at altitude of 400 ft over North Compartment 40

4.2.1.2. Thiessen polygons from photo-interpreted tree crowns

Figure 16 provides a visual display of the Thiessen polygons produced for individual tree, symbolized according to the field plot the tree was found in. Tree locations were established by manual photo-interpretation of tree crowns from 2D mosaic image produced from 52 stereo images obtained using a UAS flown at an altitude of 400 ft above the ground. Summary statistics of cumulative Thiessen areas per plot are provided in Table 2. The mean Thiessen

polygon area for each plot was then used to correlate with mean tree size per plot, in terms of basal area, volume and biomass.

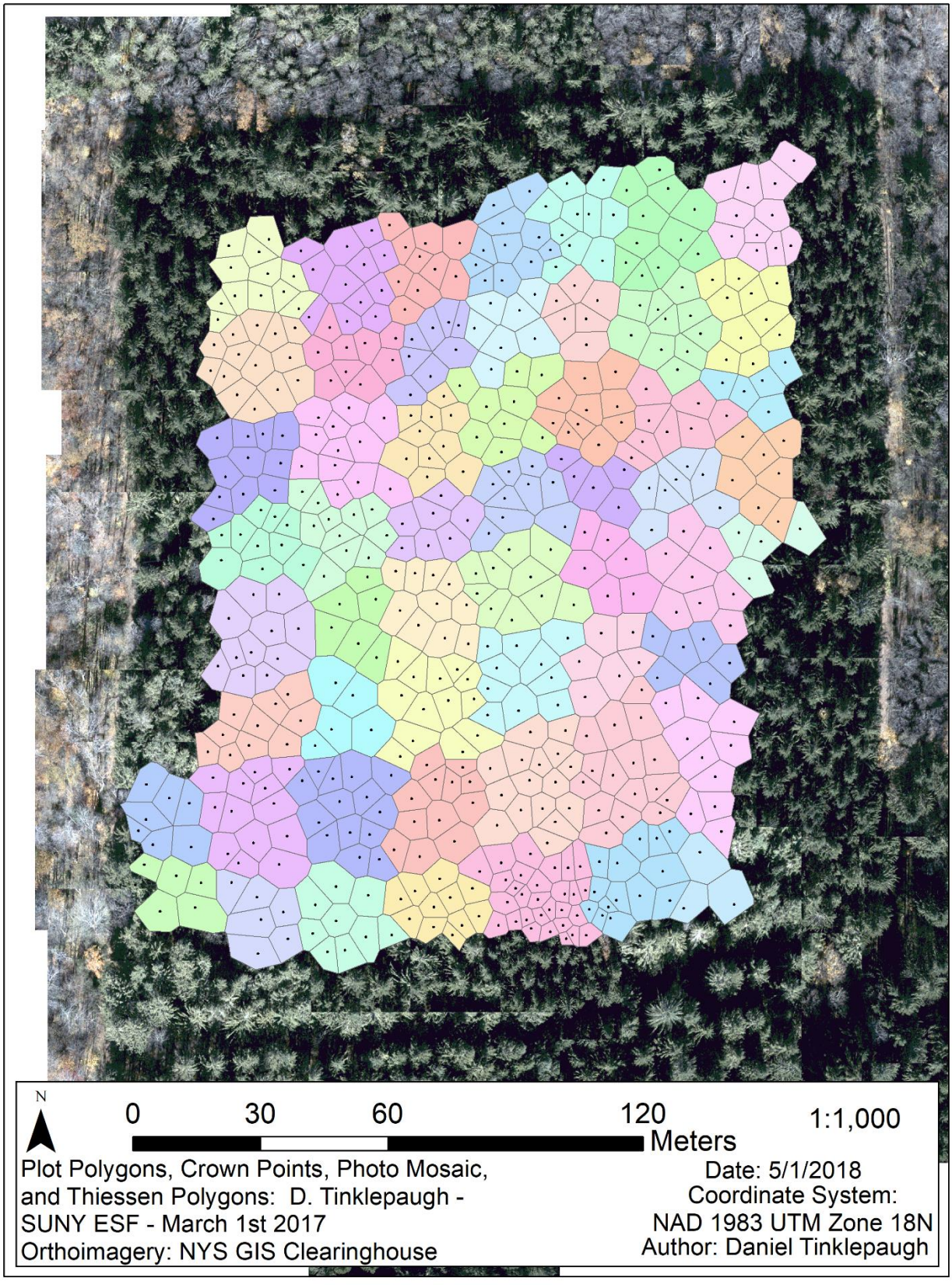

Figure 16: Distribution of Thiessen polygons among 55 interior plots.

4.2.2. Relationship between field and photo-interpreted estimates of tree counts per plot

There was a very low correlation, positive linear relationship (Figure 17) between the average number of trees per plot as measured by hand and the number of trees per plot estimated through my aerial imagery. Each data point represents one plot (both methods included), for a total of 55 points. I suspect that in areas where more trees exist, I was able to identify more trees from imagery, but both poor correlations and slopes of <1 indicates significant omission of trees based on photo-interpretation.

Plots 69 and 78 exhibit great differences between photointerpreted and field counts. Plot 69 is immediately north and adjacent to plot 78. While I generally expected to see photo counts lower than field counts, plot 69's photo count is only 16 vs. a field count of 42. Alternatively, plot 78 has a photo count of 29 vs. a field count of 17. I believe that the vast difference in counts for plot 78 come from inaccuracies in mosaic production in which an image covering a larger area was compressed into a smaller area, thereby increasing stem density in plot 78.

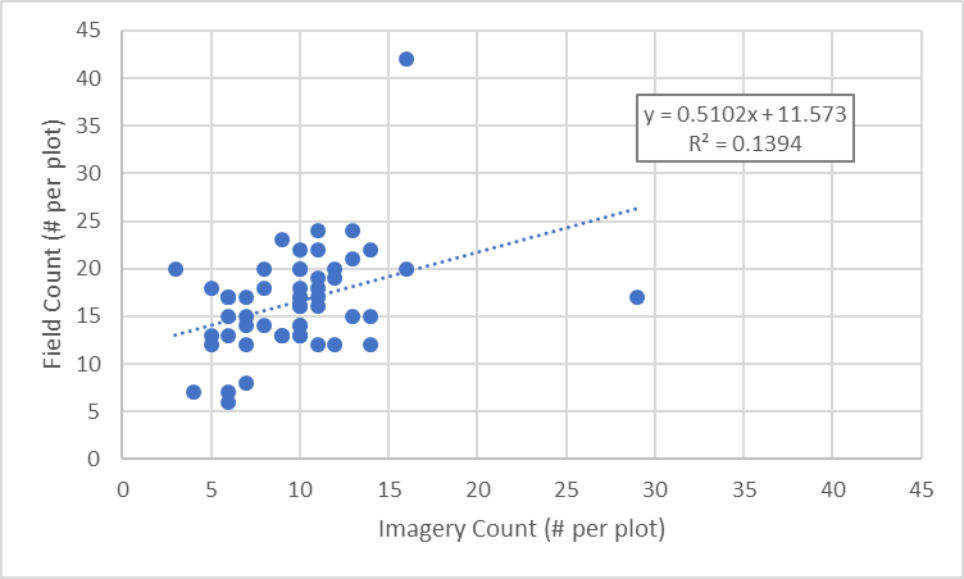

Figure 17: Scatter plot showing the relationship between field and photo-interpreted estimates of tree counts per plot.

4.2.3. Relationship between field-based mean tree basal area and photo-based mean Thiessen polygon area per plot

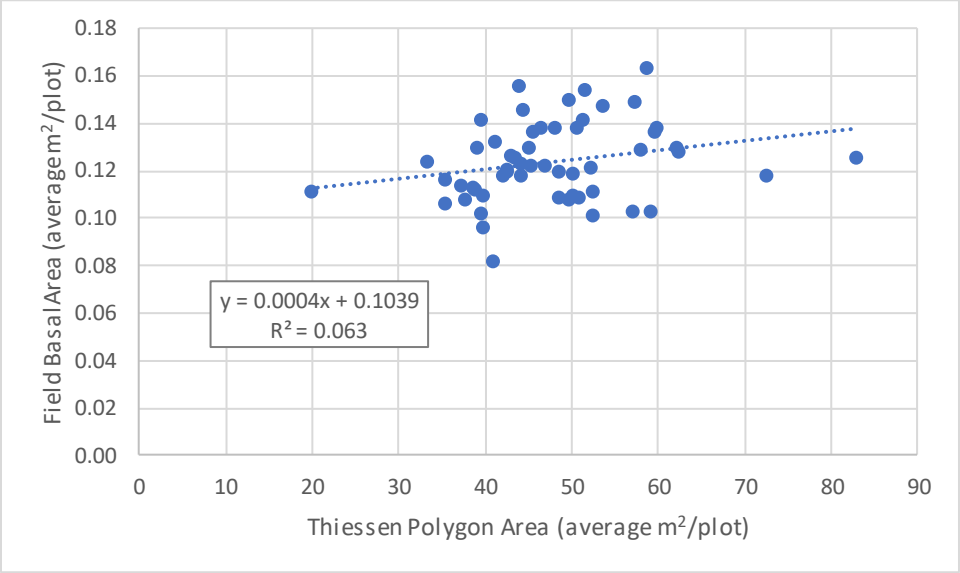

Figure 18: Scatter plot showing relationship in average tree size per plot based on mean Thiessen polygon area from photo-interpretation of tree locations and mean tree basal area from field measurements.

There was a low correlation, positive linear relationship (Figure 18) between the mean field-based basal area and photo-based mean Thiessen polygon area. It was observed that the variation in mean Thiessen areas (from 20– 80 m^2/plot) is a four-fold increase vs. basal area (0.08– 0.16 m^2/plot) is doubling. I expect that such a large variation in the x-axis will likely decrease the positivity of its relationship with the y-axis.

4.2.4. Relationship between field-based mean tree volume and photo-based mean Thiessen polygon area per plot

There was a low correlation, positive linear relationship (Figure 19) between the field stem volume and the Thiessen polygon area.

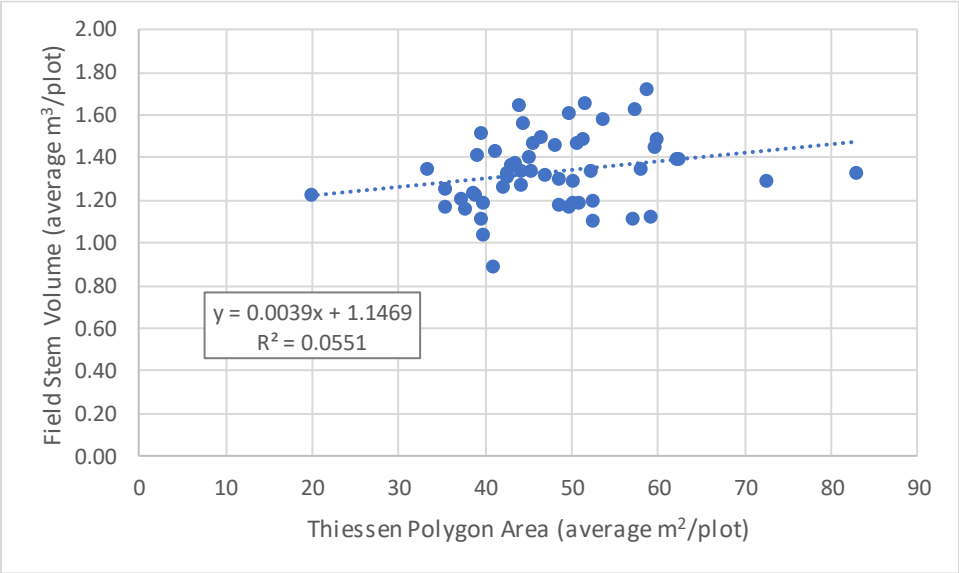

Figure 19: Scatter plot showing relationship in average tree size per plot based on mean Thiessen polygon area from photo-interpretation of tree locations and mean tree volume from field measurements.

4.2.5. Relationship between field-based mean tree biomass and photo-based mean Thiessen polygon area per plot

There was a low correlation, positive linear relationship (Figure 20) between the field biomass and the Thiessen polygon area.

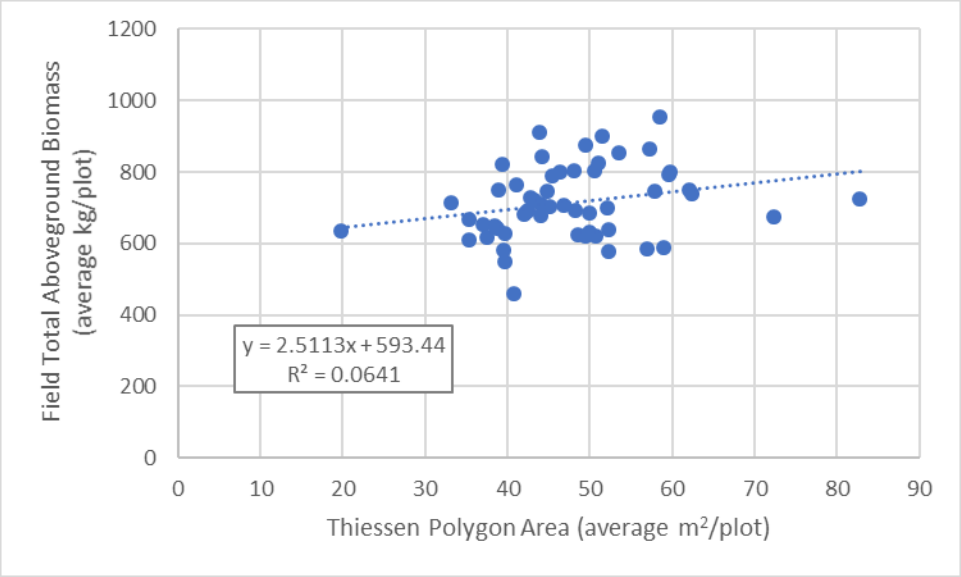

Figure 20: Scatter plot showing relationship in average tree size per plot based on mean Thiessen polygon area from photo-interpretation of tree locations and mean tree biomass from field measurements

CHAPTER 5. DISCUSSION

5.1. Photogrammetric Analysis of UAS Imagery

5.1.1. Various Software Approaches Tried

Drone Deploy, Web ODM, Pix4D, and Agisoft Photoscan are all photogrammetry software packages used to produce high quality 3D models and point clouds from geotagged 2D stereo images. Each of these programs were tested for their applicability to the Norway spruce in my study area, yet none were able to produce a coherent model from any of the missions' images.

Drone Deploy, Pix4D, and Photoscan offer free trials for a few weeks with full access to the service after the end of the trial period. WebODM, however, is completely free to use but requires that the user install a Linux Kernel onto their machine, partition their RAM, Hard Drive, and reference a few lines of Ubuntu code available in YouTube tutorials to access to the program through a web browser interface.

5.1.2. Difficulty Creating Point Cloud

It was impossible to derive a 3D image from any of the 200, 300, or 400 ft RGB datasets. My initial assumption was that aerial missions flown at the lowest suggest altitude (200 ft) would provide the best data to work with. While improved spatial resolution was naturally expected, I had not considered the extent to which parallax distortion would exist for our study area. As the sensor was flying low above a large area of trees whose heights were approximately 100 ft apiece and parts of the canopy extended nearly to the forest floor, the

75% ground sampling distance (GSD) overlap did not often capture the same object in multiple frames.

To improve the photogrammetric processing, I would recommend that one disable the feature to timestamp an image as it is taken. The timestamp is unnecessary as one may recover the time and location of a captured image through the Exchangeable image file format (Exif) metadata and impedes proper functionality in 3D image processing. More than a few of the output point clouds had a distinct region composed of white pixels clearly representing a single line of text. I believe this to be one of the greatest impediments to proper point cloud production as it was one of the few items in all images to be recognizable as the same feature yet did not in any way accurately represent the subject being photographed.

5.1.3. Difficulty in Creating Mosaic

The copy of ERDAS IMAGINE available to me included the 2D MosaicPro plugin which combines two or more orthorectified images into one continuous image. While not always seamless, the automatically generated output is significantly more useful than a large number of individual images for analysis and export purposes.

Georeferencing each image takes an average of 4 minutes to align with orthoimagery from NYS GIS Clearinghouse. With 52 images for the 400 ft flyover the whole process took about 4 hours. Georeferencing is a process by which the user designates points on two images, taken at different times over the same location, that are shared. In most cases, the user will do such a thing more than once in order to properly align the image with multiple shared points. These georeferenced images were then imported into 2D MosaicPro and a test mosaic was produced.

While covering the entire study area, I noticed that a significant portion of the mosaic contained oblique views of many trees where near-vertical perspectives were expected. Before the next run I selected an option to crop the image area by a certain percentage when selected from a folder. This function is in place to crop the borders from film-based images automatically and for many images at once. Because every mission was flown with 75% overlap between neighboring images I tested producing the mosaic with 25%, 75%, and 80% crop applied to the imported images. Doing so removed a certain amount of the edge of each image to which the fix was applied (Figure 21). In the end I decided to produce the mosaic with 80% crop because once I passed beyond this value I discovered that gaps began to open between neighboring images.

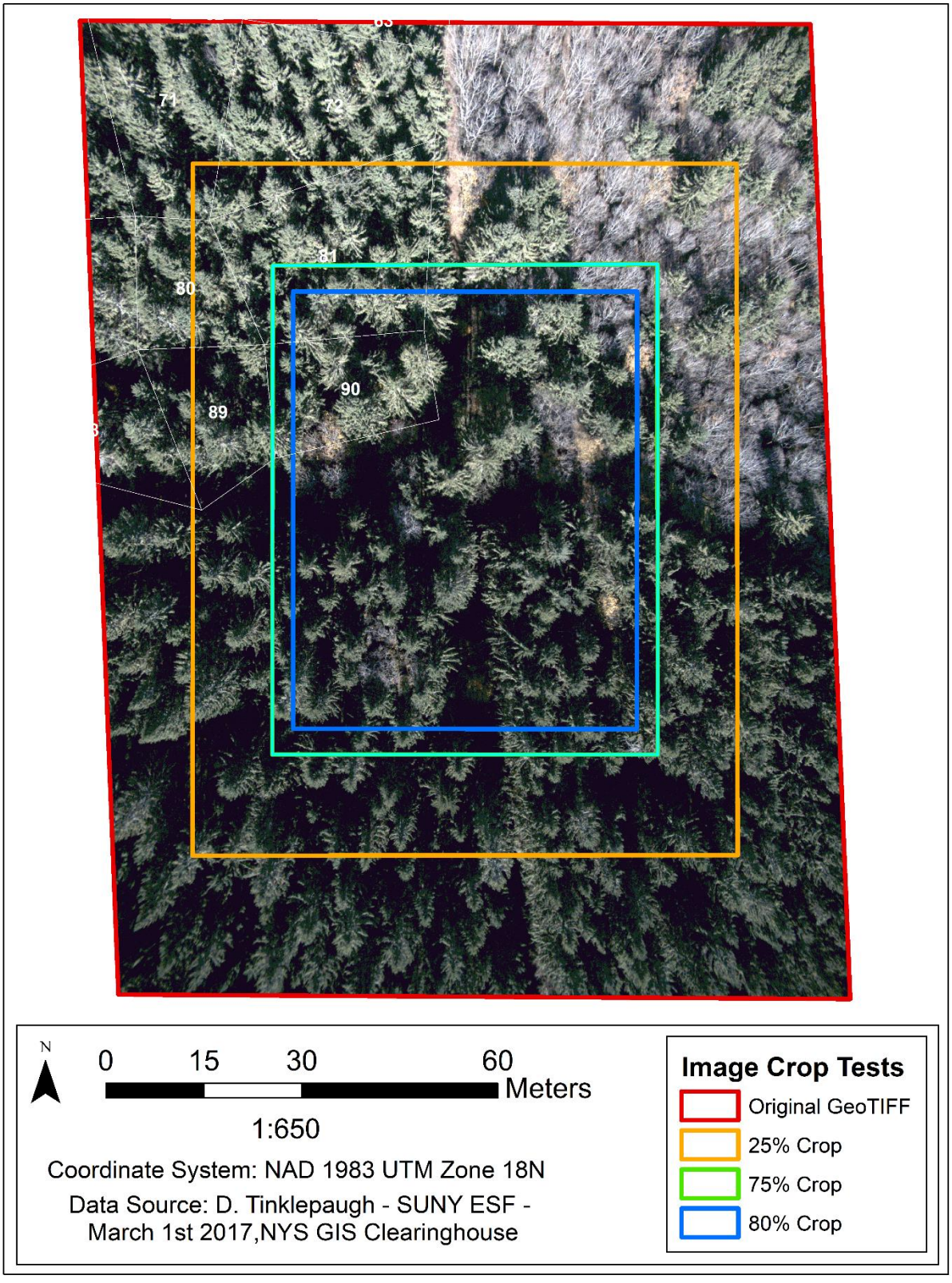

Figure 21: Illustration of how individual stereo aerial images were cropped in order to produce 2D mosaic image of the study site.

5.2. Individual Tree Extraction from Imagery

Low correlation between field measurements and photointerpretation of individual trees in nearly every situation implies that the methods outlined in this thesis are not suitable to depend on when performing aerial biomass estimation missions. However, with refined approaches and a better understanding of the limitations of the tools may prove that aerial biomass estimation is viable with low cost aerial platforms.

5.3. Removing Border Plots from Analyses

In the proper delineation of tree crowns using Thiessen polygons, plots bordering the edge of North Compartment 40 provided a unique issue: Thiessen polygons used to delineate tree crowns might be cut off if too close to this edge. Also, any tree crowns from neighboring areas might be in the study area but not a part of the Thiessen polygon layer. Therefore, 35 border plots were removed from the final analyses. This reduced the total tree count from 1,532 to 908 individuals, as well as 35 plots from analyses (Figure 22).

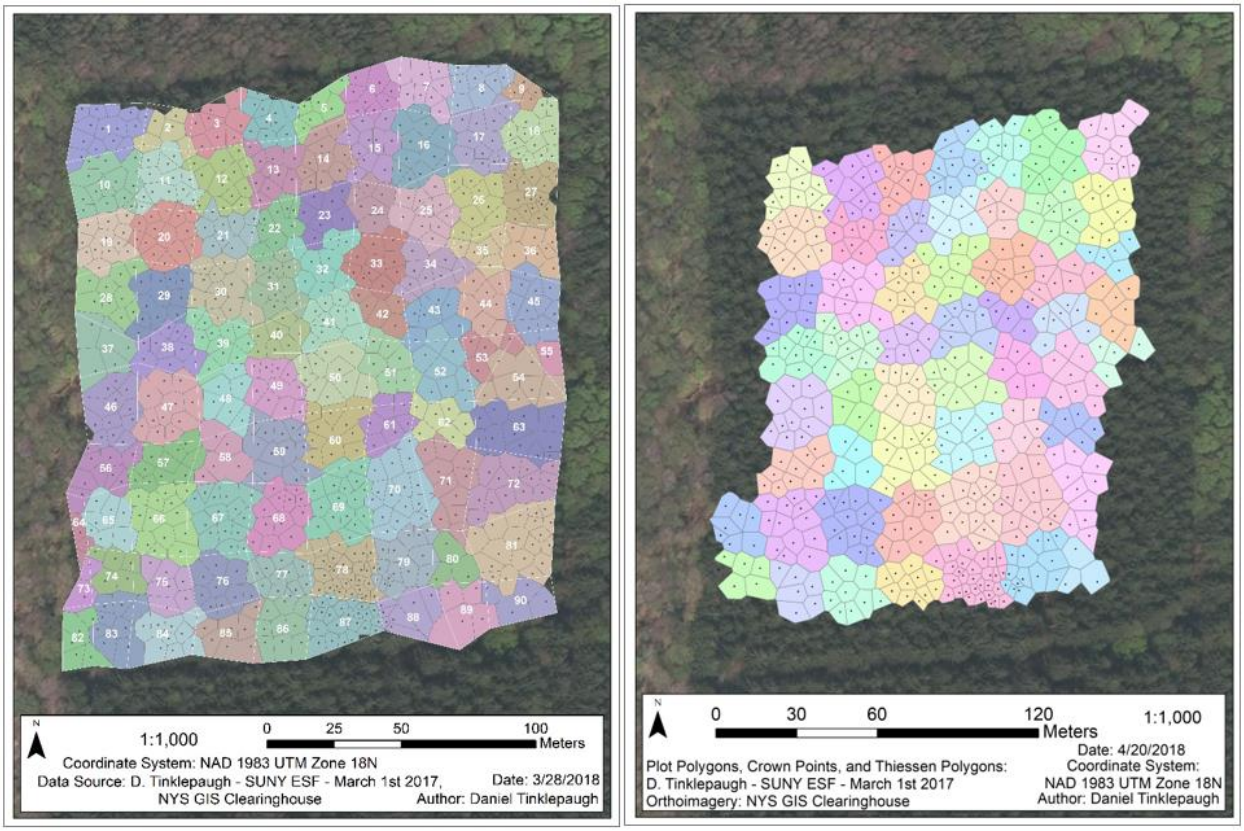

Figure 22: Comparison of the Thiessen polygon distribution with and without the border plots included.

5.4. Comparing Stem Volume Estimation between European and American Allometric Equations

While choosing an allometric equation with which to estimate stem volume for Norway spruce I considered two options: the first was an equation developed in Scandinavia and one that was developed in a region of New York State known as the Allegheny plateau. While my first intention was to use an equation developed from a population so close to my study area, I instead chose the former equation (Equation 2) rather than the latter:

$$Y = b_0 + b_1 D + b_2 D^2 + e \quad (5)$$

where *Y* equals tree volume (ft^3), *D* equals dbh (in), b_i*'s* represent regression coefficients, and *e* is an error term. As this equation estimates volume in cubic feet, all values were converted into cubic meters (m^3) for further analysis.

Because my study area contained individuals whose DBH ranged from 16.5 to 68 cm, it was decided that using an allometric equation developed from individuals whose dbh's were close to my own would mean that volume estimations for larger individuals would be closer to true values. Jokela's (Equation 5, 1986b) equation was developed from stands whose diameters ranged from 16.5 cm to 24.4 cm, whereas Muukkonnen's (Equation 2, 2007) equation was developed from a range of 10 cm to 50 cm individuals. While the two equations produced similar volume predictions within the common range of DBHs used to fit the models, extrapolation of Jokela's (1986b) polynomial equation for larger individuals appears to quickly overestimate volumes relative to Muukkonnen's (2007) equation (Figure 23).

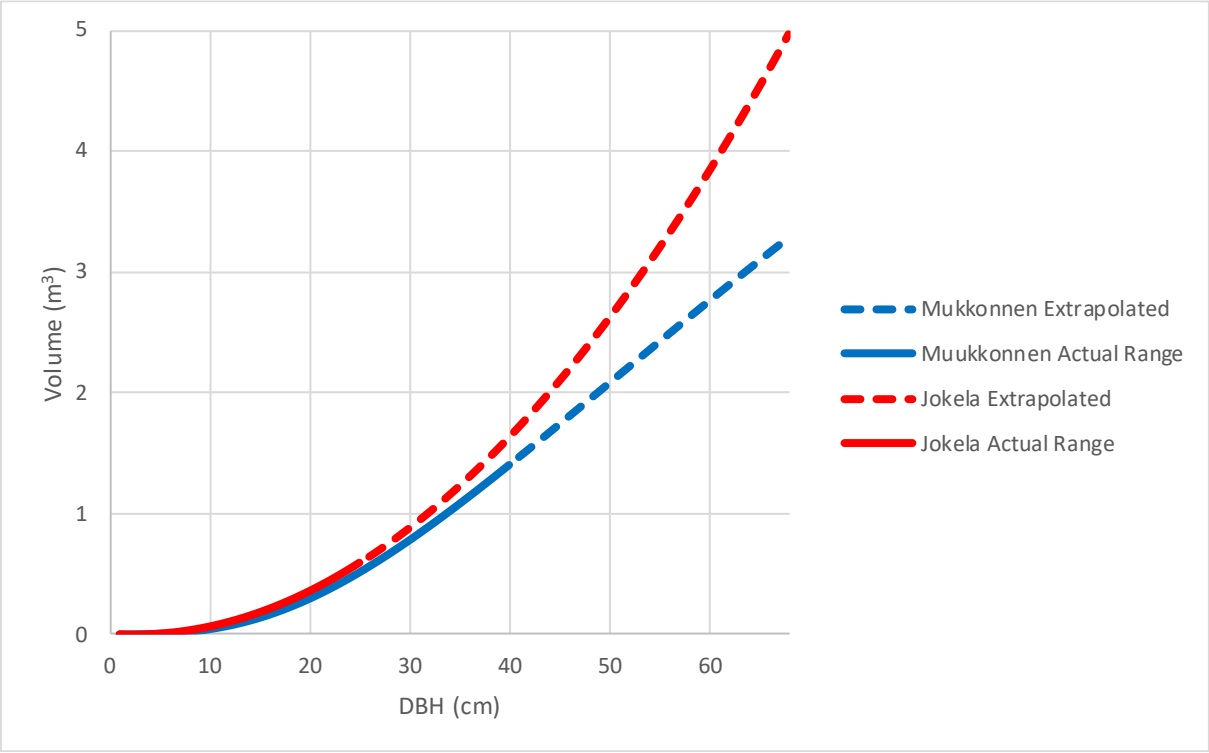

Figure 23: Comparison of the tree volume predictions between Mukkonnen (2007) and Jokela et al. (1986b) for full range of DBH encountered at the study site.

CHAPTER 6. CONCLUSIONS

Unmanned aerial systems are the future of low-cost, timely, and high-resolution data gathering for natural resources management. Their greater flexibility over traditional aerial surveying technology is strong and analytical methods used to interpret data gathered with UAS use can only improve. Although results from this research were not strong, this is likely due to first time implementation of the technology. Lessons learned from this research suggest that with refined image gathering and analysis techniques, one may be able to produce coherent 3D models of mature homogeneous forests with the tools used in this thesis. Specifically, flying at higher altitude and slower velocity to ensure stable image acquisition with a high degree of image overlap will likely improve orthomosaic and 3D point cloud creation, along with individual tree recognition.

CHAPTER 7. LITERATURE CITED

AgiSoft PhotoScan Professional (Version 1.4.2) (Software). (2018). [Internet] Available from: http://www.agisoft.com/downloads/installer/

Anderson, Karen, and K. J. Gaston. (2013) “Lightweight Unmanned Aerial Vehicles Will Revolutionize Spatial Ecology.” Frontiers in Ecology and the Environment, 11:138-146. https://doi.org/10.1890/120150

ArduPilot Dev Team (2017). Mission Planner. Version 1.3.49. [Internet] Available from: http://firmware.ardupilot.org/Tools/MissionPlanner/.

Avery, Thomas Eugene., and Harold E. Burkhart. Forest Measurements. McGraw-Hill, 1983.

Boose, E., Boose, E., Lezberg, A. L. (1998) A practical method for mapping trees using distance measurements. Ecology 79: 819-827.

Boose E., Boose E., Lezberg A. (1999) INTERPNT Software for Mapping Trees Using Distance Measurements. Harvard Forest Data Archive: HF023. [Internet] Available from: http://harvardforest.fas.harvard.edu:8080/exist/apps/datasets/showData.html?id=hf023

Brown, G.S. (1965) “Point density in stems per acre.” *New Zealand Forestry Research Notes* 38.

DroidPlanner Labs (2016). Tower App. Version 4.0.0. Google Play Store. [Internet] Available from: https://play.google.com/store/apps/details?id=org.droidplanner.android

DroneDeploy (2018). DroneDeploy. Version 2.67.0. Google Play Store. [Internet] Available from: https://www.dronedeploy.com/.

ERDAS (2014) ERDAS Imagine 2014. Hexagon Geospatial, Peachtree Corners Circle Norcross. [Internet] Available from: https://www.hexagongeospatial.com/products/power-portfolio/erdas-imagine

ESRI (2018) ArcGIS Desktop: Release 10.5. Redlands, CA: Environmental Systems Research Institute. [Internet] Available from: http://desktop.arcgis.com/en/arcmap/

Everaerts, Jürgen. (2008) "The use of unmanned aerial vehicles (UAVs) for remote sensing and mapping." *The International Archives of the Photogrammetry, Remote Sensing and Spatial Information Sciences* 37.2008: 1187-1192

Federal Aviation Administration (FAA) (2016). “Summary of Small Unmanned Aircraft Rule (Part 107).” Federal Aviation Administration, U.S. Department of Transportation, 21 June 2016, [Internet] Available from: www.faa.gov/uas/media/Part_107_Summary.pdf.

Ford, E.D. and K.A. Sorrensen. (1992) “Theory and models of inter-plant competition as a spatial process.” *In* DeAngelis, D.L. and Gross, L.J. (eds). *Individual-based models and approaches in ecology: populations, communities and ecosystems*. Routledge, Chapman and Hall, Inc., New York, NY, pp. 363-407

Franklin, S. E., Wulder, M. A., and Gerylo, G. R. (2010) “Texture Analysis of IKONOS Panchromatic Data for Douglas-Fir Forest Age Class Separability in British Columbia.” Taylor & Francis Online, International Journal of Remote Sensing, https://doi.org/10.1080/01431160120769

Gittleman, John L. (2011) “Allometry.” Encyclopedia Britannica, Encyclopedia Britannica, Inc., , [Internet] Available from: www.britannica.com/science/allometry.

Jokela E. J., K. P. Van Gurp, R. D. Briggs, and E. H. White. (1986a) “Biomass Estimation Equations for Norway Spruce in New York.” Canadian Journal of Forest Research, NRC Research Press, 1986, https://doi.org/10.1139/x86-075

Jokela, Eric J., R, D. Briggs, and E. H. White. (1986b) “Volume Equations and Stand Volumes for Unthinned Norway Spruce Plantations in New York.” SUNY College of Environmental Science and Forestry. https://academic.oup.com/njaf/article-abstract/3/1/7/4802787?redirectedFrom=PDF

MAPIR Camera. (2018). Survey2 Cameras. [Internet] Available from: www.mapir.camera/collections/survey2.

Minitab (2018). Minitab Reference Manual. Release 17.4.1. State College, PA :Minitab, [Internet] Available from: www.minitab.com.

Microsoft Excel (2016). Version 3.04. Redmond, WA, [Internet] Available from: www.microsoft.com.

Muukkonnen, P. (2007) “Generalized Allometric Volume and Biomass Equations for Some Tree Species in Europe.” European Journal of Forest Research. 126: 157. https://doi.org/10.1007/s10342-007-0168-4.

Nair, P. K. Ramachandran, Mohan, K. B., and Nair, V. D. (2009) “Agroforestry as a Strategy for Carbon Sequestration.” Journal of Plant Nutrition and Soil Science, https://doi.org/10.1002/jpln.200800030.

Pettorelli, Nathalie, J. Olav Vik, A. Mysterud, J.-M. Gaillard, C. J. Tucker, and Nils Chr. Stenseth. (2005) “Using the Satellite-Derived NDVI to Assess Ecological Responses to Environmental Change.” Trends in Ecology & Evolution, Elsevier Current Trends, www.sciencedirect.com/science/article/pii/S016953470500162X.

Pix4D (2018). Pix4D. [Internet] Available from: https://pix4d.com/

Remondino, F., L. Barazzetti, F. Nex, M. Scaioni, and D. Sarazzi. (2011) “UAV Photogrammetry For Mapping And 3d Modeling – Current Status And Future Perspectives –.” International Archives of the Photogrammetry, Remote Sensing and Spatial Information Sciences, vol. 38, 2011, pp. 1–22., [Internet] Available from: 3dom.fbk.eu/sites/3dom.fbk.eu/files/pdf/Remondino_etal_UAV2011.pdf.

Schmidt, Friedemann. (2011). Geosetter. Version 3.4.16. [Internet] Available from: http://www.geosetter.de/en/

Seibert, Sebastian, and J. Teizer. (2014) “Mobile 3D Mapping for Surveying Earthwork Projects Using an Unmanned Aerial Vehicle (UAV) System.” Automation in Construction, https://doi.org/10.1016/j.autcon.2014.01.004

Spurr, S. H. (1946). Aerial Photographs in Forestry. Technische Zentralstelle Der Deutschen Forstwirtschaft.

Tang, Lina, and G. Shao. (2015) “Drone Remote Sensing for Forestry Research and Practices.” Journal of Forestry Research. 26(4): 791-797. https://doi.org/10.1007/s11676-015-0088-y

Waharte, Sonia, and N. Trigoni. (2010) “Supporting Search and Rescue Operations with UAVs.” 2010 International Conference on Emerging Security Technologies, Canterbury, 2010, pp. 142-147. https://doi.org/10.1109/EST.2010.31.

WebODM (2018). Drone Mapping Software based on OpenDroneMapper. [Internet] Available from: https://github.com/OpenDroneMap/WebODM/

CHAPTER 8. APPENDIX

Table 3: A complete list of calculations derived from field measurements and photointerpretation.

Plot#	Field data				Photointerpretation	
	Field Count	Average Basal Area ($m^{2)}$	Average Volume ($m^{3)}$	Average Biomass (kg)	Photo Count	Average Thiessen Polygon Area ($m^{2)}$
1	20	0.163	1.734	951.8	14	--
2	16	0.116	1.232	671.1	5	--
3	19	0.118	1.283	679.0	8	--
4	21	0.107	1.169	612.9	10	--
5	15	0.118	1.266	678.3	6	--
6	17	0.118	1.262	678.7	8	--
7	16	0.127	1.375	735.4	8	--
8	15	0.104	1.134	595.2	8	--
9	20	0.081	0.875	456.0	4	--
10	18	0.131	1.418	757.5	13	--
11	20	0.106	1.169	609.0	12	35.27
12	19	0.109	1.191	628.0	12	39.72
13	18	0.102	1.111	580.4	10	39.50
14	18	0.108	1.161	617.9	11	37.56
15	14	0.118	1.263	681.5	10	42.00
16	12	0.122	1.336	699.6	11	52.10
17	16	0.122	1.340	704.1	11	45.19
18	24	0.088	0.956	502.2	13	--
19	14	0.137	1.470	793.1	12	--
20	15	0.112	1.226	642.8	14	38.74
21	13	0.141	1.512	821.5	9	39.43
22	14	0.130	1.413	749.6	8	38.90
23	17	0.138	1.472	802.5	7	50.57
24	13	0.109	1.183	625.1	6	48.50
25	16	0.138	1.462	802.9	10	48.03
26	20	0.122	1.317	705.9	10	46.86
27	40	0.091	0.994	519.3	17	--
28	17	0.135	1.470	783.3	9	--
29	19	0.132	1.428	763.7	11	41.10
30	12	0.136	1.466	788.6	12	45.50

31	13	0.113	1.236	649.3	10	38.40
32	23	0.108	1.169	619.1	9	49.50
33	13	0.118	1.268	677.6	10	44.07
34	18	0.109	1.185	622.4	8	50.75
35	12	0.138	1.497	798.8	5	46.33
36	24	0.100	1.092	571.3	7	--
37	18	0.076	0.821	427.3	5	--
38	22	0.081	0.889	459.5	10	40.76
39	24	0.113	1.206	654.0	11	37.07
40	14	0.145	1.562	844.7	7	44.22
41	13	0.156	1.646	909.8	9	43.84
42	13	0.150	1.612	874.2	5	49.43
43	12	0.154	1.651	900.0	7	51.48
44	8	0.149	1.630	865.7	7	57.19
45	20	0.125	1.356	721.0	10	--
46	21	0.103	1.102	587.7	12	--
47	22	0.101	1.108	577.9	11	52.26
48	17	0.103	1.127	588.7	6	59.00
49	14	0.125	1.376	720.1	10	43.34
50	16	0.147	1.581	855.5	10	53.45
51	17	0.128	1.395	740.6	6	62.33
52	20	0.130	1.391	750.2	8	62.13
53	7	0.138	1.490	799.3	4	59.71
54	15	0.124	1.361	715.3	7	--
55	10	0.118	1.233	682.7	1	--
56	10	0.096	1.049	547.2	9	--
57	17	0.120	1.325	689.3	10	42.30
58	18	0.118	1.288	675.9	5	72.37
59	15	0.129	1.405	747.3	13	44.87
60	17	0.110	1.192	630.1	10	49.93
61	15	0.129	1.348	747.5	6	57.81
62	17	0.111	1.198	638.6	6	52.35
63	40	0.118	1.277	676.7	11	--
64	3	0.110	1.208	626.8	3	--
65	15	0.119	1.288	683.8	7	49.99
66	21	0.120	1.300	691.2	13	48.30
67	22	0.126	1.363	728.9	14	42.78
68	24	0.120	1.314	692.4	13	42.51
69	42	0.096	1.039	547.4	16	39.71

70	20	0.123	1.342	709.5	16	44.04
71	20	0.102	1.114	586.6	10	56.89
72	31	0.124	1.343	713.5	13	--
73	8	0.108	1.183	616.1	2	--
74	7	0.136	1.449	793.1	6	59.52
75	6	0.163	1.720	955.8	6	58.50
76	13	0.141	1.490	823.3	9	51.10
77	17	0.124	1.350	713.1	11	33.13
78	17	0.111	1.226	636.4	29	19.75
79	12	0.116	1.252	668.2	14	35.34
80	20	0.125	1.334	725.1	3	82.75
81	25	0.117	1.270	676.0	18	--
82	8	0.163	1.757	947.9	5	--
83	5	0.147	1.603	854.2	9	--
84	17	0.124	1.355	714.6	11	--
85	21	0.119	1.298	683.0	7	--
86	17	0.113	1.237	651.1	10	--
87	18	0.129	1.376	749.6	22	--
88	11	0.123	1.339	706.8	7	--
89	16	0.134	1.412	776.5	4	--
90	13	0.126	1.352	730.9	4	--

Curriculum Vitae

Education

SUNY College of Environmental Sciences and Forestry (ESF), Syracuse, NY **January 2016 – Present**
Master's Degree Candidate, Graduate Program in Environmental Science;
Concentration in Environmental Monitoring and Modeling

Union College, Schenectady, NY **Earned B.S. June 2015**
Environmental Sciences Major

Professional Experience

Town of DeWitt, DeWitt, NY **May 2017 – Present**

Independent Contractor; hired to compile comprehensive geospatial data on the Town of DeWitt concerning its natural resources and open space.

SUNY ESF, Syracuse, NY **Spring Semesters 2016 & 2017**

Graduate Assistant to Professor Bevilacqua;
Instructed usage of ArcMAP to undergraduate students in weekly labs

Skills and Coursework

Coursework:

Advanced GIS
Experimental Design and ANOVA
Natural Resources Law and Policy
Landscape Ecology
Hydrology
Geodetic, Plane, and Cadastral Surveying
Principles of Remote Sensing
Probability Sampling Methods
Statistics for Environmental Sciences
Environmental and Energy Auditing
Population Ecology
Intermediate Chemistry

Computer & Technical Skills:

Expert: ArcGIS for Desktop extensions
Proficient: All Microsoft Office Extensions, Garmin ETrex GPS, Trimble Tripod GPS, QGIS
Beginner: Javascript, CSS, HTML, Python, Linux

Employment and Internships:

Town of DeWitt, Cartographic Contractor; OSI/NRI & CEA Report **May 2017 – Present**
SUNY ESF, Research Assistant; Willow Crop Field Technician **June – August 2017**
SUNY ESF, Graduate Teaching Assistant; Intro to GIT **Spring Semesters 2016 & 2017**

Professional Affiliations and Activities

GPES Representative to the Graduate Student Association (GSA) **Fall 2016 – Present**

- Attend bi-weekly meetings to allocate graduate student fees through programs, opportunities, and activities designed to enhance the graduate student experience at SUNY ESF

Attendee to Town of DeWitt Advisory Conservation Commission (DACC)

Spring 2017 – Present

- Participate in monthly meetings of local professionals and citizens to advise the town board on matters affecting the use of natural and man-made features of the Town of DeWitt.